Atmos. Chem. Phys. Discuss., doi:10.5194/acp-2016-770, 2016
Manuscript under review for journal Atmos. Chem. Phys.
Published: 5 September 2016

Atmospheric Chemistry and Physics Discussions

Assimilation of satellite NO_2 observations at high spatial resolution

Xueling Liu[1], Arthur P. Mizzi[2], Jeffrey L. Anderson[3], Inez Fung[1] and Ronald C. Cohen[1,4]

[1]Department of Earth and Planetary Science, University of California at Berkeley, Berkeley, CA, USA
[2]Atmospheric Chemistry Observation and Modeling Laboratory, National Center for Atmospheric Research, Boulder, CO, USA
[3]Institute for Mathematics Applied to Geosciences, National Center for Atmospheric Research, Boulder, CO, USA
[4]Department of Chemistry, University of California at Berkeley, Berkeley, CA, USA

Correspondence to: Ronald C. Cohen (rccohen@berkeley.edu)

Abstract. Observations of trace gases from space based instruments offer the opportunity to constrain chemical and weather forecast and reanalysis models using the tools of data assimilation. To date, attempts at assimilation of nitrogen dioxide (NO_2) satellite remote sensing have focused on updating emissions and concentrations. These initial efforts evaluated updates at length scales of ~100 km using once a day measurements from satellites with ground pixels of 13 km × 24 km or larger. In the boundary layer, NO_2 has a lifetime on the order of five hours and corresponding 1/e concentration variations near urban and point sources occur on spatial scales on the order of 50-75 km. Accurate observations and modeling of these variations require spatial resolution of order 4 km. In addition, because of the short lifetime, NO_2 variations are more strongly coupled to short time scale meteorological parameters than longer lived chemicals such as CO or CO_2. In the next few years, we anticipate the launch of several instruments with ~3 km spatial resolution. In addition, some of these instruments will be in geostationary orbits and thus have hourly revisit times. In anticipation of these instruments, we investigate the potential of high space and time resolution column measurements to serve as constraints on urban NO_x emissions using a geostationary observation simulator coupled to a data assimilation system. We find that constraints on emissions are strongest in regions with high emissions and are most effective when coupled to hourly assimilation of meteorological observations. We find that errors in the meteorological fields result in unrecoverable biases in the updated emissions confirming a conjecture that simultaneous meteorology and chemical assimilation is essential to accurate description of the emissions and chemistry.

1 Introduction

Weather and climate act in concert with emissions to establish the concentrations of chemicals and aerosols in the boundary layer. To improve forecasts of exposure and understand the factors that affect public health and the productivity of agriculture and animal husbandry, we require accurate models of both emissions and the boundary layer meteorology to define the surface layer concentrations that determine the exposure of humans, animals and plants. There remain substantial uncertainties in even the best models of emissions and even more so in the best models of boundary layer dynamics (for

Atmos. Chem. Phys. Discuss., doi:10.5194/acp-2016-770, 2016
Manuscript under review for journal Atmos. Chem. Phys.
Published: 5 September 2016

Atmospheric Chemistry and Physics Discussions

example, Hu et al., 2010). Current uncertainties in the surface NO_2 emission inventories in the U.S. are thought to be on the order of 50% (Krotkov et al., 2016; Travis et al., 2016). Comparable uncertainties affect estimates of the planetary boundary layer (PBL) height and mixing rates that redistribute emissions from the surface (Kretschmer et al., 2012, 2014; Jiang et al., 2013; Lauvaux and Davis, 2014).

Over the last decade, data assimilation techniques have been used to constrain model forecasts and reanalysis of atmospheric constituents (Arellano Jr. et al., 2007; Edwards et al., 2009; Claeyman et al., 2011; Lahoz et al., 2012; Pagowski and Grell, 2012; Bowman, 2013; Gaubert et al., 2014; Hache et al., 2014; Saide et al., 2014; Zoogman et al., 2014; Barré et al., 2015; Bousserez et al., 2015; Mizzi et al., 2016). Assimilation of chemicals can be extended to optimize model inputs, such as emissions, thereby providing insight into how to improve the processes that govern the model performance (Chatterjee et al., 2012; Cui et al., 2015; Elbern et al., 2007; Guerrette and Henze, 2015; Huang et al., 2014; Koohkan et al., 2013; Miyazaki et al., 2012b; Turner et al., 2015).

To date most efforts to incorporate satellite remote sensing in data assimilation have focused on long-lived chemicals such as CO, CH_4 or CO_2 on the regional and continental scale of emissions. Processes that govern variability of emissions within an urban center require new approaches that use high spatial and temporal resolution models and observations. NO_2 has a lifetime of only a few hours and thus exhibits concentration changes that are substantial on spatial scales of 50-75 km. Observations of variations in NO_2 are thus uniquely suited to study emissions and meteorology at the scales of cities. Averaged measurements of NO_2 have been shown to be promising for evaluation of absolute emissions and trends (Russell et al., 2012; Miyazaki et al., 2016) as well as providing information on the coupling of boundary layer winds to chemical lifetime (Beirle et al., 2011; Valin et al., 2013). Current space based instruments have resolutions that are too low to provide direct information on lifetimes and emissions from a single overpass. Instead, analyses have focused on averages of the data that wash out some of the key details about emission location and chemical lifetime.

New instruments with spatial resolution of a few kilometers will soon change that situation. The TROPOspheric Monitoring Instrument (TROPOMI, launch date of 2016) will be the first to provide spatial resolution sufficient to observe these NO_2 changes on a single overpass. TROPOMI will view the atmosphere from low earth orbit and provide one image per day. We also anticipate the launch of three geostationary satellites, the Geostationary Environmental Monitoring Spectrometer (GEMS), the Tropospheric Emissions: Monitoring of POllution (TEMPO) and Sentinel-4, which will provide observations at higher temporal resolution with hourly repeat at locations in Asia, North America and Europe, respectively (Lee et al., 2010; Chance et al., 2013; Gulde et al., 2014). The spatial resolution of these new low earth orbit (LEO) and Geostationary (GEO) instruments will be sufficient to provide ~10 samples within the advection distance that is determined by the chemical lifetime of NO_2. This dense sampling will permit characterization of multi-exponential or non-exponential behavior where current analyses are typically forced to assume single exponential decay. To take full advantage of these measurements in a data assimilation system, we will need to model the NO_2 column at similar spatial resolution. This is both because the spatial scales of important variation in atmospheric plumes are on the order of 4 km and because of the steep non-linearity in the lifetime of NO_2 as a function of the NO_2 concentration. For example, biases of 34% (3.3 to 5.0 molecules/cm^2) are found in

Atmos. Chem. Phys. Discuss., doi:10.5194/acp-2016-770, 2016
Manuscript under review for journal Atmos. Chem. Phys.
Published: 5 September 2016

Atmospheric Chemistry and Physics Discussions

the modeled average NO_2 column over Los Angeles at resolutions of 96 km compared with 12 km. For a point source, such as a power plant, model convergence is observed only at a grid resolution of 4 km or smaller (Valin et al., 2011).

In this study, we describe a high spatial and temporal resolution chemical ensemble data assimilation system that simultaneously adjusts meteorological and atmospheric composition state variables and emissions on scales consistent with the temporal scale of NO_x evolution. We use that forecast/assimilation system to investigate: (i) the ability of TEMPO NO_2 observations to accurately constrain NO_x emissions, and (ii) the sensitivity of the NO_x emission estimate to meteorological uncertainties. Our long-term goal is to estimate hour-to-hour variations in NO_x emissions at the scale of model grid point resolution (3 km) and to use these variations to understand the processes controlling the emissions. The remainder of this paper is organized as follows: In section 2, we describe the forecast/data assimilation system, the system setup, observations, and the TEMPO NO_2 simulator – the simulation of column NO_2 that would be observed by TEMPO. In section 3, we describe the experimental design including a series of assimilation experiments that guide the optimization of the modeling. In section 4, we explore the sensitivity of the optimized NO_x emissions to uncertainty in meteorological variables and assess the benefits of hourly observations of NO_2 column and meteorological parameters as constraints on emissions. We then discuss the results and provide insights into the potential accuracy of NO_2 emission fields derived from geostationary NO_2 observations. We conclude in section 5.

2 The data assimilation system

The data assimilation system used here consists of the following elements: the forecast model, the assimilation engine, and observations of meteorological and chemical states to be assimilated.

2.1 WRF-Chem and DART

The core meteorological and chemical forecast model is the regional online chemical transport model WRF-Chem v3.4.1 (www2.acd.ucar.edu/wrf-chem). The model domain is a one-way nest with an outer domain of 12 km resolution covering western North America and an inner domain of 3 km resolution focused on the city of Denver, CO (Figure 1). The 3 km domain is 660 km by 840 km. The model has 30 vertical levels between the surface and an upper boundary of 100 mbar and 10 levels within the boundary layer (~1.5 km). Simulations of meteorology on the outer domain are initialized and constrained at the lateral boundary by the North American Regional Reanalysis (NARR) data from National Centers for Environmental Prediction (NCEP). The NARR data have a native horizontal resolution of 32 km with 45 pressure levels and 3 h temporal resolution. The chemical simulation on the outer domain is initialized with an idealized profile setting provided by WRF-Chem. After a spin-up time of 40 hours on the outer domain, the inner domain simulation is initialized and constrained through one-way nesting in both meteorology and chemistry.

Anthropogenic emissions for WRF-Chem are from the National Emission Inventory (NEI) 2011 for a typical July weekday at native 4×4 km resolution. Biogenic emissions are calculated online with the simulation results by Model of Emissions of

Atmos. Chem. Phys. Discuss., doi:10.5194/acp-2016-770, 2016
Manuscript under review for journal Atmos. Chem. Phys.
Published: 5 September 2016

Atmospheric Chemistry and Physics Discussions

Gases and Aerosols from Nature (MEGAN). Fire emissions are not included. We use the RADM2 gas phase chemical mechanism for its simplicity (Stockwell et al., 1990).

WRF-Chem/DART (data assimilation research testbed) is a regional multivariate data assimilation system developed by the National Center for Atmospheric Research (NCAR) to analyze meteorological variables and chemical variables simultaneously (Mizzi et al., 2016). We use the Ensemble Adjustment Kalman Filter (EAKF) in DART to analyze the states with an ensemble size of 30. Details of the EAKF algorithm and its implementation in DART are documented in (Anderson, 2001; Anderson and Collins, 2007; Anderson et al., 2009). In this study the system is modified and implemented to assimilate synthetic TEMPO NO_2 column observations. The state variables include the NO_2 concentration, 3D winds (U, V, W), temperature (T), surface pressure, specific humidity (QVAPOR), cloud ice and cloud water. As emissions are not prognostic variables of the forecast model, a state augmentation approach is applied to include emissions in the state variables (Aksoy, 2006).

We generate the initial chemical ensemble by adding the perturbations to the mean state of the fine domain forecast. In the ensemble method the generated ensemble should represent the error statistics of the initial guess of the model state (Evensen, 2003). The correlation between perturbations of chemical state variables is modeled by a simple isotropic exponential decay function with a characteristic correlation length of 50 km. We use the WRF Data Assimilation (WRFDA) system (http://www2.mmm.ucar.edu/wrf/users/wrfda) to generate the initial ensemble of meteorological variables.

A challenge for updating the emissions in the augmented state vector is the absence of an emission forecast model to evolve the emission variables forward in time. The bottom-up inventory to be optimized provides hourly-resolved emissions for each model grid point. Instead of treating the emission variables of each hour at a specific location as independent parameters, we adjust the first guess (prior) of the emission at the current time (t+1) based on the posterior emission of the previous hour (time t). First we calculate the scaling factor at time t as the ratio of the posterior emission to the prior at t. Then as a forecast step we obtain the new prior emission at t+1 by multiplying the original prior at t+1 with the scaling factor from t. This prescription enables us to derive spatial 2-D emission scaling factors which play the role of an emission forecast model.

2.2 Covariance localization

In ensemble methods the correlations among spatially remote variables in the prior ensemble are regarded as spurious correlations due to the small ensemble size (30). To compensate for this under-sampling issue, spatial localization is introduced to dampen the prior correlations based on the distance between the observed/modeled state variables (Houtekamer and Mitchell 2001). In this study, we apply the fifth-order distance-dependent function from Gaspari and Cohn (GC) 1999 to reduce the spurious impact of observations on spatially remote state variables. The scaling distance in the GC function is defined by a half-width parameter, two times which is the distance where the GC function goes to zero. With a data assimilation window of one hour and a maximum wind speed of 3~5 m/s, an observation of column NO_2 contains information about emissions that occurred within the last hour if they are within 10 km. We use the half-width distance in

Atmos. Chem. Phys. Discuss., doi:10.5194/acp-2016-770, 2016
Manuscript under review for journal Atmos. Chem. Phys.
Published: 5 September 2016

spatial localization as 10 km. We chose the 10 km distance based on sensitivity experiments with localization distance of 5 km, 10 km, 20 km and 50 km. Because of the high density of TEMPO NO_2 observations (2×4.5 km), the update of chemical state variables is mostly determined by the local observations.

Similar to the concept of spatial localization, variable localization techniques have been introduced (Arellano Jr. et al., 2007) to reduce spurious correlations among observations and different types of state variables. For example, for CO_2 flux estimation, Kang et al. (2011) suggest that the performance of data assimilation using a variable localization that zeros out the prior error covariance between meteorological variables and CO_2 flux is better than using a standard full covariance approach. We also find that the meteorological observations introduce spurious correlations with chemical observations that degrade performance. We thus avoid the impact of meteorological observations on chemical variables and vice versa.

2.3 Synthetic meteorological and chemical observations

Observations assimilated in the system include conventional meteorological observations and NO_2 trace gas retrievals from TEMPO. For meteorological observations, we assimilated simulated NCEP Automated Data 20 Processing (ADP) upper air and surface observations (PREPBUFR observations). They included air temperature, sea level pressure, surface winds, dew point temperature, sea surface temperature, and upper level winds from various observing platforms.

The GEOstationary Coastal and Air Pollution Events (GEO-CAPE) mission (Fishman et al., 2012) aims at improving our understanding of both coastal ecosystems and air-quality from regional to continental scales. As the first phase of the GEO-CAPE implementation, TEMPO, launch date circa 2019, will provide hourly measurements of NO_2, HCHO, tropospheric ozone, aerosols, and cloud parameters during the daytime. TEMPO will measure solar back scattered light in the UV-Vis spectral range. Implemented on a geostationary platform, TEMPO retrievals will achieve hourly observations of NO_2 vertical column density (VCD) at a native spatial resolution of 2×4.5 km during the day-lit period. TEMPO's high spatiotemporal resolution will allow a more detailed assessment of emission inventories, e.g. urban scale and large power plant NO_2 emissions and mobile emissions that show significant spatial and temporal variations due to urban transit patterns, than is possible with existing LEO observations.

As the TEMPO has not been launched yet, we generate synthetic TEMPO NO_2 observations by simulating the instrument's observing characteristics. We carried out a model run, i.e. a forward integration of WRF-CHEM for the period from July 2nd to July 7th 2014 with NO_2 emissions specified by NEI 2011 ('truth'). We calculate a layer dependent Box-Air Mass Factor (BAMF) representing the sensitivity of the retrieved NO_2 in a specific layer to the true value in the atmosphere. The BAMF of NO_2, as an optically thin absorber, is a vector and determines the measurement sensitivity to NO_2 molecules at 35 pressure levels. In the calculation of BAMFs, we follow the latest version of the NASA standard product retrieval (Level 2, Version 2.1, Collection 3) algorithm (Bucsela et al., 2013) assuming the TEMPO measurement has similar characteristics as OMI. We assume clear-sky conditions for all observing scenes. Cloudy-sky scenes affect only the number of observations available as the cloudy scenes are usually discarded in the data filtering process. The elements of the BAMF vector are computed as a function of solar zenith angle, viewing zenith angle, relative azimuth angle, terrain reflectivity, terrain

Atmos. Chem. Phys. Discuss., doi:10.5194/acp-2016-770, 2016
Manuscript under review for journal Atmos. Chem. Phys.
Published: 5 September 2016

Atmospheric Chemistry and Physics Discussions

pressure, atmospheric pressure level and the NO_2 profile (Bucsela et al., 2013). The viewing parameters are computed by simulating viewing geometry based on the location of ground pixels in relation to the observing instrument. The other parameters are sampled from the model run and have 3×3 km native spatial resolution. All the parameters have an hourly frequency consistent with the TEMPO temporal observing pattern. Consequently, the NO_2 profile with high-spatial-temporal resolution captures the diurnal variation of NO_2 and its urban-rural contrast. This contrast is essential to accurate interpretation of the measured spectrum (Russell et al., 2011; Laughner et al., 2016).

To generate synthetic TEMPO data, the modeled 3-D concentration fields from the nature run (NR, see in section 3) are sampled in as similar a manner to the planned TEMPO measurements as the transport model permits: using the computed BAMF vertically; hourly frequency; 2×4.5 km nadir resolution and variations following the Earth's curvature horizontally. Figure 2 shows an example of spatial distribution of TEMPO data over Denver, CO.

We describe the observation error as a relative value (σ_{rel}) and a random draw from a Gaussian distribution to avoid using a fixed value. The magnitude of the mean uncertainty of the NO_2 column is different between clean and polluted areas (Boersma et al., 2004). We follow their categorization of clean vs polluted regions and summarize the mean and standard deviations of Gaussian distributions for each scenario in Table 3. For polluted regions, we give a mean uncertainty of 7.5%, which is lower than the 35% minimum in the OMI NO_2 retrieval. First, most of these errors are systematic, affecting comparison of different cities but have smaller variation across a single, small area scene of observations. Second, a relatively lower observation error improves the efficiency of data assimilation and helps to examine the sensitivity to other parameters, such as meteorological uncertainties. Finally, as TEMPO is expected to be operational no sooner than 2018, it is reasonable to expect the retrieval error dominated by AMF in polluted regions will be reduced as a result of future improvements in AMF simulation (Laughner et al., 2016). The synthetic observations assimilated are obtained by sampling the NR using the TEMPO observation simulator and adding observation error as $y^{obs} = N(y^{tr}, \sigma^2)$, where σ is the observation error standard deviation computed as $\sigma = y^{tr} \cdot \sigma_{rel}$.

3 Assimilation experiments

We begin by performing observing system simulation experiments (OSSEs) in the context of a perfect model. We consider the NR as the true atmosphere and sample meteorological and NO_2 observations from the NR. The control run (CR) is a parallel model calculation to the NR and suffers from imperfect model input and parametrization. The differences between the NR and the CR in this study are the emission inputs and the initial conditions for the meteorology. We begin by creating a NR and a CR simulation on the outer domain of 12 km resolution (d01) without assimilating observations using a simulation setup as described above in section 2a. We impose a difference to the CR by using emissions that are scaled to be 70% of the NR emissions. We apply the identical forecast model (WRF-Chem) for both the NR and the AR to isolate the behavior of the ensemble filter algorithm from the influence of the model errors. Then the NR and the CR on the inner domain of 3km (d02) is initialized from the corresponding d01 simulation respectively at 06:00 local time (LT) on July 2nd

Atmos. Chem. Phys. Discuss., doi:10.5194/acp-2016-770, 2016
Manuscript under review for journal Atmos. Chem. Phys.
Published: 5 September 2016

2014. At the point of initialization, the NR and CR on d02 share the same meteorological field and differ in NO_x concentrations due to different emission inputs. Our next step is to generate an ensemble from the CR. We choose 30 ensemble members. We use WRFDA to generate an ensemble in meteorological variables (Barker et al., 2012). For chemical states, we give an ensemble in NO_x emissions and concentrations using the method described above in section 2a. The forecast of the CR ensemble is the prior estimate of the states and will be combined with the observations in the assimilation cycle to yield the posterior states. By comparing the posterior emissions with the "true emission", we evaluate the data assimilation performance. We run assimilation experiments from 08:00 LT to 17:00 LT on July 2nd with an assimilation window of one hour. We assimilate the NO_2 observations each hour and we vary the frequency of assimilation of the meteorological observations.

Our first assimilation experiments were designed to evaluate the benefits of meteorology assimilation, as shown in Table 1. In all experimental runs, we bias the CR initial emissions to be 30% below the reference model and examine the ability of the assimilation to recover the reference emissions. First, a reference assimilation run (REF) is conducted without including the meteorological ensemble so that the NR and the CR ensemble have identical meteorological simulations. This shows the limits to constraints on emissions by examining an ideal case that assumes no uncertainties associated with meteorology. In the next calculation, labelled as the BIAS-MET run, we add the difference to the meteorological initial condition between the NR and the CR by replacing the d02 NR meteorological field with one member of the CR ensemble generated by WRFDA. For winds, the bias of CR compared with the modified NR is ±1.5 m/s in Denver. We only assimilate NO_2 observations in this BIAS-MET simulation. This calculation is used to assess the impact of biased meteorology on emission estimates that do not incorporate meteorological assimilation. Finally, we assess the sensitivity of the emission estimates to meteorological assimilation using calculations with joint assimilation of meteorology and chemistry. We include both meteorological and chemical ensembles, labelled as ENS. We focus on the horizontal wind assimilation in particular because it has the most influence on the NO_2 forecast among all meteorological variables. We have three ENS runs that differ in the temporal frequency of the wind observations assimilated. The ENS-O case mimics the availability of upper level wind observations in reality with wind observations available at the 17:00 LT assimilation cycle each day. In ENS-T we duplicate the wind observations by adding a second assimilation of winds at 8:00LT. In ENS-H we assimilate the wind observations at the same hourly steps as the chemical observations.

4 Results

We begin our analysis by comparing the assimilation results with the NR. Table 2 summarizes the statistics of the root mean square (RMS) errors and uncertainties in posterior zonal wind and NO_x emissions averaged over the last four hourly assimilation cycles when the emission estimation results become stable. The RMS error at the analysis time step is computed by $\sqrt{\sum_i^n (x_i^a - x_i^t)^2/n}$, where x_i^a and x_i^t are the posterior and true states respectively at the ith model grid point, and n is the total number of grid points of interest. For the wind variable, the grid points of interest are all the points located within a sub-

Atmos. Chem. Phys. Discuss., doi:10.5194/acp-2016-770, 2016
Manuscript under review for journal Atmos. Chem. Phys.
Published: 5 September 2016

Atmospheric Chemistry and Physics Discussions

model space as shown in Figure 4, containing the lowest 10 model levels vertically. Because NO_x is located mostly in the boundary layer, the NO_2 transport error is determined by the meteorological errors in the lowest 10 model levels. For NO_x emission variables, the grid points of interest are categorized as urban emission points with emissions greater than 80 mol/(km^2·hr) and suburban emission points with emissions between 30 and 80 mol/(km^2·hr). Our analysis does not include emissions below 30 mol/(km^2·hr) because the observations over such low emission regions have large uncertainty and emissions are not constrained by the observations.

With no meteorological observations assimilated (BIAS-MET), the errors in zonal and meridional winds grow from ~1.4 m/s to as large as 2.1 m/s as the forecast advances. The resulting NO_2 transport errors, together with emission errors, lead to the model-observation NO_2 mismatch. The assimilation does not recognize the wind field errors and attributes all of the error to emissions. As a result, the BIAS-MET calculation exhibits the largest RMS errors, and the bias in the estimate of emissions grows to be larger than the initial uncertainty of 41.70 mol/(km^2·hr). The assimilation is incapable of recovering the correct emissions when the winds are biased.

Assimilation of meteorology in ENS runs reduces RMS errors in wind by more than 50% compared with BIAS-MET calculation, as shown in Table 2. ENS-H shows a slightly lower RMS error than the ENS-O or ENS-T due to more frequent observations assimilated. The differences in wind errors among the three ENS runs are small. But the uncertainties in the predicted wind are very different among ENS runs. Figure 3 shows the time evolution of wind uncertainty represented by the ensemble spread.

The covariance between NO_x emissions and column NO_2 is lost when the wind spread is large, degrading the ability of the assimilation to recover the true emissions. In Table 2 we compare the correlation of emission variables against synthetic TEMPO NO_2 observations for suburban and urban regions. We average the correlation statistics within the localization radius. The correlation is strongest (R^2 = 0.76~0.77) in the REF run and degrades with increasing uncertainties in winds. The correlation also remains strong (with R^2 above 0.70) in the run with biased meteorology, even though the posterior NO_x emission differs from the emissions in the NR.

Urban NO_2 observations show higher correlation with emissions than suburban observations (Table 2). Uncertainty in winds and emissions both contribute to the concentration uncertainty. The wind uncertainty varies little over the city and the region east of the mountains, and increases over the mountains, as shown in Figure 4. The emission uncertainty is larger at urban points and smaller at suburban, and therefore dominates the overall concentration uncertainty in urban regions. Not surprisingly, urban observations better preserve the correlation with emissions when the noise from wind is lower.

Experiments ENS-O, ENS-T and ENS-H explore how the efficiency of this ensemble data assimilation to constrain emissions varies with the ensemble used for estimating the correlation between emissions and observations. Figure 5 shows scatter plots of posterior emissions versus the true emissions for different treatments of the meteorological uncertainties. The grey dashed lines are a reference with zero bias and slope equal to unity. The regression slopes improve from 0.7 (prior value) to 0.99 (REF) and 1.04 (ENS-H). The REF and ENS-H runs recover the true emissions at the scale of a model grid cell at grid points with emissions above 50 mol/(km^2·hr) for each experiment with exceptional fidelity. High correlation

Atmos. Chem. Phys. Discuss., doi:10.5194/acp-2016-770, 2016
Manuscript under review for journal Atmos. Chem. Phys.
Published: 5 September 2016

Atmospheric Chemistry and Physics Discussions

coefficients between the analyzed and reference emissions (R^2 > 0.94) are found for all calculations except the one with biased meteorology where the R^2 is low (0.31) and the fitted slope is not meaningful. The performance degrades substantially in the ENS-O calculation where a regression slope of 1.21 is observed.

As a result of well-formed constraints from the observations on urban emissions, the emission estimation results show lower relative RMS error and uncertainty in the urban than in the suburban region as shown in Table 2. We divide the RMS error statistics by the truth as normalization. ENS-H shows largest error reduction after REF. But urban and suburban areas show differences in the uncertainty of estimated emissions. The prior emissions in all AR experiments are initialized with an initial uncertainty of ~35%, similar to the emission uncertainty used for global NO_x emission estimates (Miyazaki et al., 2012a). For urban emissions, without the contribution of transport errors, the REF run gives urban emission estimation with a mean uncertainty of 6% (83% uncertainty reduction). The emission uncertainty in the ENS runs increases due to the transport uncertainty contribution. Compared with other ENS runs, ENS-H shows the lowest uncertainty (8%) in the posterior urban emissions with an uncertainty reduction of 77%, when the transport uncertainty is constrained by hourly meteorological observations. For suburban emissions, the uncertainties are larger than urban emissions as a result of degraded ensemble correlation with observations. This indicates that the emissions in urban centers can be estimated with higher confidence than the emissions in suburban regions.

From the perspective of emission mitigation policy, it is informative to provide the range of the uncertainty in such top-down emission estimates. We analyzed the emission estimates and the uncertainty of total emissions at the city scale in Denver. The emission analyses in all grid points (urban + suburban) are aggregated as the total mean with the total uncertainty calculated by error propagation. Figure 6 shows the probability distribution function of the total emissions estimate. The truth for the total emissions falls in the 95% confidence interval of the REF, ENS-H and ENS-T runs, which shows increasing degrees of uncertainty. The ENS-O and BIAS-MET runs show larger uncertainty levels, with 95% confidence intervals that do not overlap with the truth, which indicates that they cannot provide reliable emissions estimates.

5 Summary and conclusions

In this study, we demonstrate the ability to estimate NO_x emissions by assimilating NO_2 and meteorological observations into a regional data assimilation system comprised of WRF-Chem and DART-EAKF. Such an ensemble-based data assimilation system is appealing for regional chemical transport studies as it allows the flexibility and efficiency to assimilate observations with various scales and of various chemical species. This is especially true, at present, in light of the availability of future long-term multi-species observations from satellite, such as GEO-CAPE and TROPOMI.

One of the goals of this work is to investigate the optimal strategy to estimate NO_x emissions. Previous work has shown that NO_x concentrations and columns vary at fine scales necessitating high spatiotemporal resolution to make use of them in the assimilation. In the coupled chemical and meteorological data assimilation system, we apply an OSSE framework to estimate NO_x emissions in Denver by jointly assimilating observation of meteorological variables as well as future TEMPO NO_2

columns. We show that emission inversion experiments using a model with "perfect" transport physics but with unresolved errors in initial meteorological fields result in NO_2 transport errors, leading to the failure to recover the true emission. When the transport errors are well constrained, future TEMPO NO_2 observations will enable us to constrain surface emissions on a city scale. In this way, the simultaneous analysis of chemical and meteorological states provides robust estimates of emissions and characterizes the uncertainty in those estimates.

To constrain the errors in meteorological variables, we include both chemical and meteorological variables in the analyzed states but zero out the covariance between chemical and meteorological states. Therefore, the optimization of emissions relies only on its covariance with concentration variables. We find that when transport uncertainties are involved, preserving the chemical covariance is essential in order to obtain effective constraints on emissions. Even if the posterior wind shows small RMS errors relative to the truth, the uncertainty in the wind grows rapidly with time in the absence of meteorological observations. The wind uncertainty dampens the chemical covariance so that the TEMPO NO_2 observations have little impact on the emissions. Our results show that our ENS-H run solves the problem of chemical covariance damping by frequent, i.e. hourly, assimilation of wind observations to reduce wind uncertainty, resulting in the best performance in recovering true emissions by reducing 51% of initial errors. We expect further improvements by assimilating meteorological observations with higher frequency and spatial coverage.

The emissions optimization scheme used in this study assumes no error in the diurnal variation of emissions, which enables us to optimize the emission scaling factors with hourly frequency. For future work, if there is a large uncertainty in the temporal variability, the emissions at different time steps can be treated as independent state variables to allow the possibility of updating the prior temporal pattern of emissions.

Finally, we note that the methodology developed in this study can also be applied to emissions estimates of other chemical species or time-evolving parameters. For chemical species with longer chemical lifetimes, care should be taken in constraining the errors in transport and boundary conditions and preserving chemical covariance, as emission-induced forcing will be less dominant.

Acknowledgements. The authors gratefully acknowledge support from the NASA Grants NNX10AR36G, and NNX15AE37G. We thank N. Collins (NCAR/IMAGe) and T. Hoar (NCAR/IMAGe) for the assistance with DART. We would like to acknowledge high-performance computing support from Yellowstone (ark:/85065/d7wd3xhc) provided by NCAR's Computational and Information Systems Laboratory, sponsored by the National Science Foundation.

Atmos. Chem. Phys. Discuss., doi:10.5194/acp-2016-770, 2016
Manuscript under review for journal Atmos. Chem. Phys.
Published: 5 September 2016

Atmospheric Chemistry and Physics Discussions

References

Anderson, J., Hoar, T., Raeder, K., Liu, H., Collins, N., Torn, R. and Avellano, A.: The Data Assimilation Research Testbed: A Community Facility, Bull. Am. Meteorol. Soc., 90(9), 1283–1296, doi:10.1175/2009BAMS2618.1, 2009.

Anderson, J. L.: An Ensemble Adjustment Kalman Filter for Data Assimilation., Mon. Weather Rev. Dec2001, 129(12), 2001.

Anderson, J. L. and Collins, N.: Scalable Implementations of Ensemble Filter Algorithms for Data Assimilation, J. Atmos. Ocean. Technol., 24(8), 1452–1463, doi:10.1175/JTECH2049.1, 2007.

Arellano Jr., A. F., Raeder, K., Anderson, J. L., Hess, P. G., Emmons, L. K., Edwards, D. P., Pfister, G. G., Campos, T. L. and Sachse, G. W.: Evaluating model performance of an ensemble-based chemical data assimilation system during INTEX-B field mission, Atmos. Chem. Phys., 7(21), 5695–5710, doi:10.5194/acp-7-5695-2007, 2007.

Barker, D., Huang, X.-Y., Liu, Z., Auligné, T., Zhang, X., Rugg, S., Ajjaji, R., Bourgeois, A., Bray, J., Chen, Y., Demirtas, M., Guo, Y.-R., Henderson, T., Huang, W., Lin, H.-C., Michalakes, J., Rizvi, S. and Zhang, X.: The Weather Research and Forecasting Model's Community Variational/Ensemble Data Assimilation System: WRFDA, Bull. Am. Meteorol. Soc., 93(6), 831–843, doi:10.1175/BAMS-D-11-00167.1, 2012.

Barré, J., Gaubert, B., Arellano, A. F. J., Worden, H. M., Edwards, D. P., Deeter, M. N., Anderson, J. L., Raeder, K., Collins, N., Tilmes, S., Francis, G., Clerbaux, C., Emmons, L. K., Pfister, G. G., Coheur, P.-F. and Hurtmans, D.: Assessing the impacts of assimilating IASI and MOPITT CO retrievals using CESM-CAM-chem and DART, J. Geophys. Res. Atmos., n/a–n/a, doi:10.1002/2015JD023467, 2015.

Beirle, S., Boersma, K. F., Platt, U., Lawrence, M. G. and Wagner, T.: Megacity emissions and lifetimes of nitrogen oxides probed from space., Science, 333(6050), 1737–9, doi:10.1126/science.1207824, 2011.

Boersma, K. F., Eskes, H. J. and Brinksma, E. J.: Error analysis for tropospheric NO_2 retrieval from space, J. Geophys. Res., 109(D4), D04311, doi:10.1029/2003JD003962, 2004.

Bousserez, N., Henze, D. K., Rooney, B., Perkins, A., Wecht, K. J., Turner, A. J., Natraj, V. and Worden, J. R.: Constraints on methane emissions in North America from future geostationary remote sensing measurements, Atmos. Chem. Phys. Discuss., 15(13), 19017–19044, doi:10.5194/acpd-15-19017-2015, 2015.

Bowman, K. W.: Toward the next generation of air quality monitoring: Ozone, Atmos. Environ., 80, 571–583, doi:10.1016/j.atmosenv.2013.07.007, 2013.

Bucsela, E. J., Krotkov, N. A., Celarier, E. A., Lamsal, L. N., Swartz, W. H., Bhartia, P. K., Boersma, K. F., Veefkind, J. P., Gleason, J. F. and Pickering, K. E.: A new stratospheric and tropospheric NO_2 retrieval algorithm for nadir-viewing satellite instruments: applications to OMI, Atmos. Meas. Tech., 6(10), 2607–2626, doi:10.5194/amt-6-2607-2013, 2013.

Chance, K., Liu, X., Suleiman, R. M., Flittner, D. E., Al-Saadi, J. and Janz, S. J.: Tropospheric emissions: monitoring of pollution (TEMPO), in SPIE Optical Engineering + Applications, edited by J. J. Butler, X. (Jack) Xiong, and X. Gu, p. 88660D, International Society for Optics and Photonics., 2013.

Chatterjee, A., Michalak, A. M., Anderson, J. L., Mueller, K. L. and Yadav, V.: Toward reliable ensemble Kalman filter estimates of CO_2 fluxes, J. Geophys. Res. Atmos., 117(22), 1–17, doi:10.1029/2012JD018176, 2012.

Claeyman, M., Attié, J.-L., Peuch, V.-H., El Amraoui, L., Lahoz, W. A., Josse, B., Ricaud, P., von Clarmann, T., Höpfner, M., Orphal, J., Flaud, J.-M., Edwards, D. P., Chance, K., Liu, X., Pasternak, F. and Cantié, R.: A geostationary thermal infrared sensor to monitor the lowermost troposphere: O_3 and CO retrieval studies, Atmos. Meas. Tech., 4(2), 297–317, doi:10.5194/amt-4-297-2011, 2011.

Cui, Y. Y., Brioude, J., McKeen, S. a., Angevine, W. M., Kim, S.-W., Frost, G. J., Ahmadov, R., Peischl, J., Bousserez, N., Liu, Z. and Ryerson, T. B.: Top-down estimate of methane emissions in California using a mesoscale inverse modeling technique: The South Coast Air Basin, J. Geophys. Res. Atmos., 120, 6698–6711, doi:10.1002/2014JD023002, 2015.

Edwards, D. P., Arellano, A. F. and Deeter, M. N.: A satellite observation system simulation experiment for carbon monoxide in the lowermost troposphere, J. Geophys. Res., 114(D14), D14304, doi:10.1029/2008JD011375, 2009.

Elbern, H., Strunk, A., Schmidt, H. and Talagrand, O.: Emission rate and chemical state estimation by 4-dimensional variational inversion, Atmos. Chem. Phys., 7(14), 3749–3769, doi:10.5194/acp-7-3749-2007, 2007.

Evensen, G.: The Ensemble Kalman Filter: theoretical formulation and practical implementation, Ocean Dyn., 53(4), 343–367, doi:10.1007/s10236-003-0036-9, 2003.

Fishman, J., Iraci, L. T., Al-Saadi, J., Chance, K., Chavez, F., Chin, M., Coble, P., Davis, C., DiGiacomo, P. M., Edwards, D., Eldering, A., Goes, J., Herman, J., Hu, C., Jacob, D. J., Jordan, C., Kawa, S. R., Key, R., Liu, X., Lohrenz, S., Mannino, A., Natraj, V., Neil, D., Neu, J., Newchurch, M., Pickering, K., Salisbury, J., Sosik, H., Subramaniam, A., Tzortziou, M., Wang, J. and Wang, M.: The United States' Next Generation of Atmospheric Composition and Coastal Ecosystem Measurements: NASA's Geostationary Coastal and Air Pollution Events (GEO-CAPE) Mission, Bull. Am. Meteorol. Soc., 93(10), 1547–1566, doi:10.1175/BAMS-D-11-00201.1, 2012.

Gaubert, B., Coman, A., Foret, G., Meleux, F., Ung, A., Rouil, L., Ionescu, A., Candau, Y. and Beekmann, M.: Regional scale ozone data assimilation using an ensemble Kalman filter and the CHIMERE chemical transport model, Geosci. Model Dev., 7(1), 283–302, doi:10.5194/gmd-7-283-2014, 2014.

Guerrette, J. J. and Henze, D. K.: Development and application of the WRFPLUS-Chem online chemistry adjoint and WRFDA-Chem assimilation system, Geosci. Model Dev., 8(6), 1857–1876, doi:10.5194/gmd-8-1857-2015, 2015.

Gulde, S. T., Kolm, M. G., Smith, D. J., Maurer, R., Sallusti, M., Bagnasco, G. and Introduction, I.: Sentinel 4: a geostationary imaging uvn spectrometer for air quality monitoring – status of design, performance and development, in International Conference on Space Optics, vol. 16., 2014.

Hache, E., Attié, J.-L., Tourneur, C., Ricaud, P., Coret, L., Lahoz, W. A., El Amraoui, L., Josse, B., Hamer, P., Warner, J., Liu, X., Chance, K., Höpfner, M., Spurr, R., Natraj, V., Kulawik, S., Eldering, A. and Orphal, J.: The added value of a visible channel to a geostationary thermal infrared instrument to monitor ozone for air quality, Atmos. Meas. Tech., 7(7), 2185–2201, doi:10.5194/amt-7-2185-2014, 2014.

Hu, X.-M., Nielsen-Gammon, J. W. and Zhang, F.: Evaluation of Three Planetary Boundary Layer Schemes in the WRF Model, J. Appl. Meteorol. Climatol., 49(9), 1831–1844, doi:10.1175/2010JAMC2432.1, 2010.

Huang, M., Bowman, K. W., Carmichael, G. R., Chai, T., Pierce, R. B., Worden, J. R., Luo, M., Pollack, I. B., Ryerson, T. B., Nowak, J. B., Neuman, J. A., Roberts, J. M., Atlas, E. L. and Blake, D. R.: Changes in nitrogen oxides emissions in California during 2005-2010 indicated from top-down and bottom-up emission estimates, J. Geophys. Res. Atmos., 119(22), 12,928–12,952, doi:10.1002/2014JD022268, 2014.

Jiang, Z., Jones, D. B. A., Worden, H. M., Deeter, M. N., Henze, D. K., Worden, J., Bowman, K. W., Brenninkmeijer, C. A. M. and Schuck, T. J.: Impact of model errors in convective transport on CO source estimates inferred from MOPITT CO retrievals, J. Geophys. Res. Atmos., 118(4), 2073–2083, doi:10.1002/jgrd.50216, 2013.

Kang, J.-S., Kalnay, E., Liu, J., Fung, I., Miyoshi, T. and Ide, K.: "Variable localization" in an ensemble Kalman filter: Application to the carbon cycle data assimilation, J. Geophys. Res., 116(D9), D09110, doi:10.1029/2010JD014673, 2011.

Koohkan, M. R., Bocquet, M., Roustan, Y., Kim, Y. and Seigneur, C.: Estimation of volatile organic compound emissions for Europe using data assimilation, Atmos. Chem. Phys., 13(12), 5887–5905, doi:10.5194/acp-13-5887-2013, 2013.

Kretschmer, R., Gerbig, C., Karstens, U. and Koch, F.-T.: Error characterization of CO_2 vertical mixing in the atmospheric transport model WRF-VPRM, Atmos. Chem. Phys., 12(5), 2441–2458, doi:10.5194/acp-12-2441-2012, 2012.

Kretschmer, R., Gerbig, C., Karstens, U., Biavati, G., Vermeulen, a., Vogel, F., Hammer, S. and Totsche, K. U.: Impact of optimized mixing heights on simulated regional atmospheric transport of CO_2, Atmos. Chem. Phys., 14(14), 7149–7172, doi:10.5194/acp-14-7149-2014, 2014.

Krotkov, N. a., McLinden, C. a., Li, C., Lamsal, L. N., Celarier, E. a., Marchenko, S. V., Swartz, W. H., Bucsela, E. J., Joiner, J., Duncan, B. N., Boersma, K. F., Veefkind, J. P., Levelt, P. F., Fioletov, V. E., Dickerson, R. R., He, H., Lu, Z. and Streets, D. G.: Aura OMI observations of regional SO_2 and NO_2 pollution changes from 2005 to 2015, Atmos. Chem. Phys. Discuss., 15(19), 26555–26607, doi:10.5194/acpd-15-26555-2015, 2015.

Lahoz, W. A., Peuch, V.-H., Orphal, J., Attié, J.-L., Chance, K., Liu, X., Edwards, D., Elbern, H., Flaud, J.-M., Claeyman, M. and Amraoui, L. El: Monitoring Air Quality from Space: The Case for the Geostationary Platform, Bull. Am. Meteorol. Soc., 93(2), 221–233, doi:10.1175/BAMS-D-11-00045.1, 2012.

Laughner, J. L., Zare, A. and Cohen, R. C.: Effects of daily meteorology on the interpretation of space-based remote sensing of NO_2, Atmos. Chem. Phys. Discuss., (July), 1–27, doi:10.5194/acp-2016-536, 2016.

Lauvaux, T. and Davis, K. J.: Planetary boundary layer errors in mesoscale inversions of column-integrated CO_2 measurements, J. Geophys. Res. Atmos., 119(2), 490–508, doi:10.1002/2013JD020175, 2014.

Lee, S., Hong, Y., Song, C.-K., Lee, J., Choi, W.-J., Kim, D., Moon, K.-J. and Kim, J.: Plan of Korean Geostationary Environment Satellite over Asia-Pacific region, EGU Gen. Assem. 2010, 12, 7595 [online] Available from: http://adsabs.harvard.edu/abs/2010EGUGA..12.7595L, 2010.

Miyazaki, K., Eskes, H. J. and Sudo, K.: Global NOx emission estimates derived from an assimilation of OMI tropospheric NO_2 columns, Atmos. Chem. Phys., 12(5), 2263–2288, doi:10.5194/acp-12-2263-2012, 2012a.

Miyazaki, K., Eskes, H. J., Sudo, K., Takigawa, M., van Weele, M. and Boersma, K. F.: Simultaneous assimilation of satellite NO_2, O_3, CO, and HNO_3 data for the analysis of tropospheric chemical composition and emissions, Atmos. Chem. Phys. Discuss., 12(7), 16131–16218, doi:10.5194/acpd-12-16131-2012, 2012b.

Miyazaki, K., Eskes, H., Sudo, K., Boersma, K. F., Bowman, K. and Kanaya, Y.: Decadal changes in global surface NO_x emissions from multi-constituent satellite data assimilation, Atmos. Chem. Phys. Discuss., 0(2), 1–48, doi:10.5194/acp-2016-529, 2016.

Mizzi, A. P., Arellano Jr., A. F., Edwards, D. P., Anderson, J. L. and Pfister, G. G.: Assimilating compact phase space retrievals of atmospheric composition with WRF-Chem/DART: a regional chemical transport/ensemble Kalman filter data assimilation system, Geosci. Model Dev., 9(3), 965–978, doi:10.5194/gmd-9-965-2016, 2016.

Pagowski, M. and Grell, G. A.: Experiments with the assimilation of fine aerosols using an ensemble Kalman filter, J. Geophys. Res. Atmos., 117(D21), n/a–n/a, doi:10.1029/2012JD018333, 2012.

Russell, A. R., Perring, A. E., Valin, L. C., Bucsela, E. J., Browne, E. C., Wooldridge, P. J. and Cohen, R. C.: A high spatial resolution retrieval of NO_2 column densities from OMI: method and evaluation, Atmos. Chem. Phys., 11(16), 8543–8554, doi:10.5194/acp-11-8543-2011, 2011.

Russell, A. R., Valin, L. C. and Cohen, R. C.: Trends in OMI NO_2 observations over the United States: effects of emission control technology and the economic recession, Atmos. Chem. Phys., 12(24), 12197–12209, doi:10.5194/acp-12-12197-2012, 2012.

Saide, P. E., Kim, J., Song, C. H., Choi, M., Cheng, Y. and Carmichael, G. R.: Assimilation of next generation geostationary aerosol optical depth retrievals to improve air quality simulations, Geophys. Res. Lett., 9188–9196, doi:10.1002/2014GL062089.Received, 2014.

Stockwell, W. R., Middleton, P., Chang, J. S. and Tang, X.: The second generation regional acid deposition model chemical mechanism for regional air quality modeling, J. Geophys. Res., 95(D10), 16343, doi:10.1029/JD095iD10p16343, 1990.

Travis, K. R., Jacob, D. J., Fisher, J. a., Kim, P. S., Marais, E. a., Zhu, L., Yu, K., Miller, C. C., Yantosca, R. M., Sulprizio, M. P., Thompson, A. M., Wennberg, P. O., Crounse, J. D., St. Clair, J. M., Cohen, R. C., Laugher, J. L., Dibb, J. E., Hall, S. R., Ullmann, K., Wolfe, G. M., Pollack, I. B., Peischl, J., Neuman, J. a. and Zhou, X.: NO_x emissions, isoprene oxidation pathways, vertical mixing, and implications for surface ozone in the Southeast United States, Atmos. Chem. Phys. Discuss., (2), 1–32, doi:10.5194/acp-2016-110, 2016.

Turner, A. J., Jacob, D. J., Wecht, K. J., Maasakkers, J. D., Lundgren, E., Andrews, A. E., Biraud, S. C., Boesch, H., Bowman, K. W., Deutscher, N. M., Dubey, M. K., Griffith, D. W. T., Hase, F., Kuze, A., Notholt, J., Ohyama, H., Parker, R., Payne, V. H., Sussmann, R., Sweeney, C., Velazco, V. A., Warneke, T., Wennberg, P. O. and Wunch, D.: Estimating global and North American methane emissions with high spatial resolution using GOSAT satellite data, Atmos. Chem. Phys., 15(12), 7049–7069, doi:10.5194/acp-15-7049-2015, 2015.

Valin, L. C., Russell, A. R., Hudman, R. C. and Cohen, R. C.: Effects of model resolution on the interpretation of satellite NO_2 observations, Atmos. Chem. Phys., 11(22), 11647–11655, doi:10.5194/acp-11-11647-2011, 2011.

Valin, L. C., Russell, A. R. and Cohen, R. C.: Variations of OH radical in an urban plume inferred from NO_2 column measurements, Geophys. Res. Lett., 40(9), 1856–1860, doi:10.1002/grl.50267, 2013.

Zoogman, P., Jacob, D. J., Chance, K., Worden, H. M., Edwards, D. P. and Zhang, L.: Improved monitoring of surface ozone by joint assimilation of geostationary satellite observations of ozone and CO, Atmos. Environ., 84, 254–261, doi:10.1016/j.atmosenv.2013.11.048, 2014.

Atmos. Chem. Phys. Discuss., doi:10.5194/acp-2016-770, 2016
Manuscript under review for journal Atmos. Chem. Phys.
Published: 5 September 2016

Atmospheric Chemistry and Physics Discussions

Table 1. The experimental set up of each assimilation run. The three ensemble runs assimilate chemical observations every hour, and differ in the temporal availability of meteorological observations assimilated. ENS-O assimilates the standard meteorological observations from NCEP only once, which is only available at the 9th assimilation cycle. In ENS-T the met observations are assimilated twice, in the 1st and 9th assimilation cycles. In ENS-H the met observations are assimilated each hourly cycle.

Experiment	Met Assim	Chem Assim	Time of met observation	note	Chemical observation
REF	No	Yes	No	Truth met	Each cycle
BIAS-MET	No	Yes	No	Biased met	Each cycle
ENS-O	Yes	Yes	Cycle 9	Met ensemble	Each cycle
ENS-T	Yes	Yes	Cycle 1 and 9	Met ensemble	Each cycle
ENS-H	Yes	Yes	Each cycle	Met ensemble	Each cycle

Table 2. The statistics averaged over the last four cycles for wind (U, V) in the planetary boundary layer, NO_x emissions and chemical correlation of emission with synthetic TEMPO column NO_2 observations.

			REF	ENS-H	ENS-T	ENS-O	BIAS-MET
U (m/s)	RMSE		0	0.83	1.03	1.07	2.14
	1-σ uncertainty		0	0.68	1.47	1.82	0
V (m/s)	RMSE		0	0.77	0.95	1.04	2.10
	1-σ uncertainty		0	0.72	1.33	1.72	0
NO_x Emission (%)	RMSE/truth	Suburban	13	18	29	25	100
		Urban	12	17	21	29	80
	1-σ uncertainty/ truth	Suburban	20	27	34	36	44
		Urban	6	8	11	12	20
Correlation	Suburban		0.76	0.60	0.33	0.08	0.72
	Urban		0.77	0.71	0.45	0.33	0.81

Table 3. Relative observation uncertainty in synthetic TEMPO NO_2 column for each scenario.

Type	NO_2 column	Gaussian distribution
Clean	$<0.3\times10^{15}$ molec. com^{-2}	N (200%, 100%)
Polluted	$>=0.3\times10^{15}$ molec. com^{-2}	N (7.5%, 2.5%)

Atmos. Chem. Phys. Discuss., doi:10.5194/acp-2016-770, 2016
Manuscript under review for journal Atmos. Chem. Phys.
Published: 5 September 2016

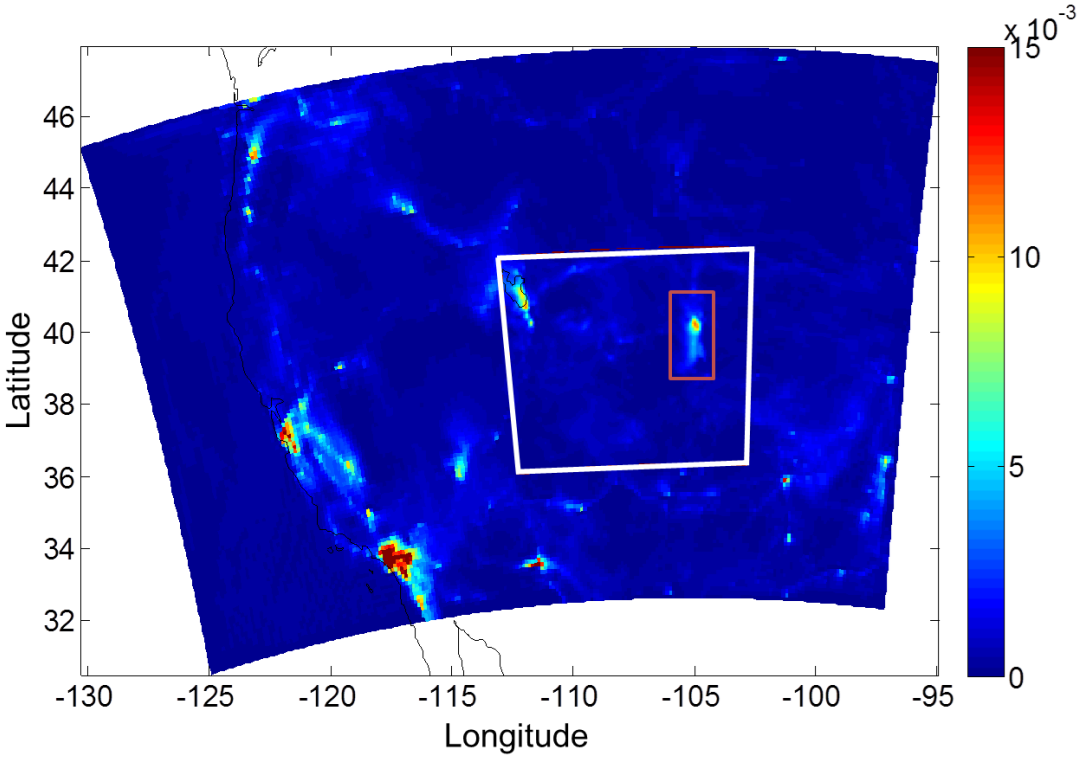

Figure 1. Model domain setup with 12 km outer domain and 3 km inner domain (white square). Data assimilation is performed on the inner domain. Meteorological observations on the inner domain are assimilated. TEMPO NO_2 observations inside the red rectangle are assimilated.

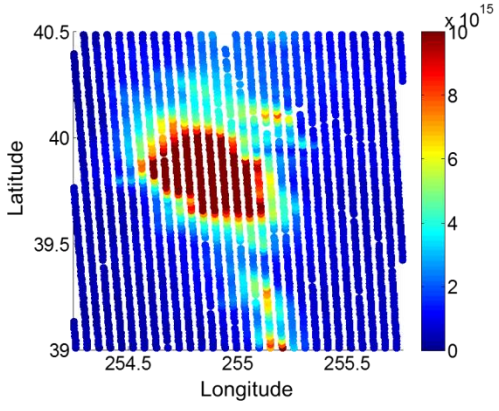

Figure 2. Example of synthetic TEMPO NO_2 column observations over Denver, CO at 17:00 LT July 2nd in 2014.

Atmos. Chem. Phys. Discuss., doi:10.5194/acp-2016-770, 2016
Manuscript under review for journal Atmos. Chem. Phys.
Published: 5 September 2016

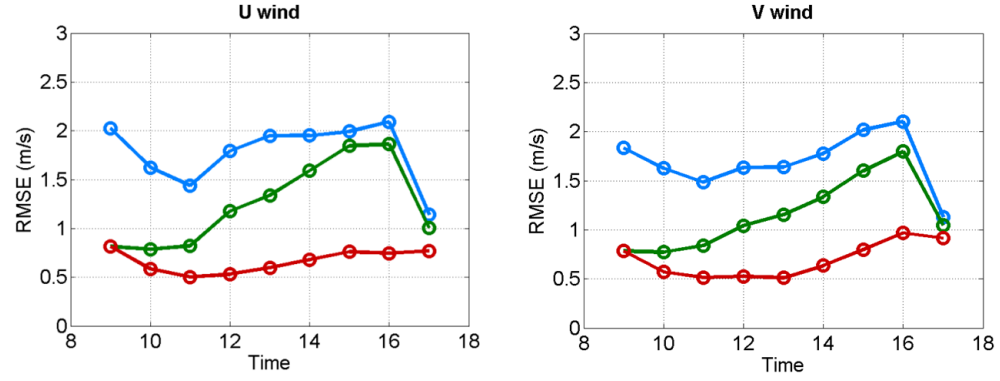

Figure 3. Time evolution of posterior wind spread on July 2nd 2014 for ENS-O (blue), ENS-T (green) and ENS-H (red).

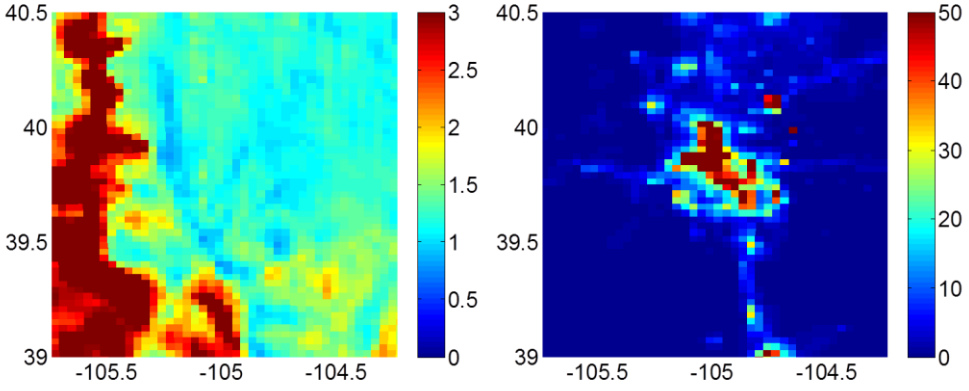

Figure 4. The prior uncertainty of zonal wind (m/s) and NO_x emissions (mol/(km^2·hr)). Longitude and latitude are marked on the x- and y- axes, respectively.

Atmos. Chem. Phys. Discuss., doi:10.5194/acp-2016-770, 2016
Manuscript under review for journal Atmos. Chem. Phys.
Published: 5 September 2016

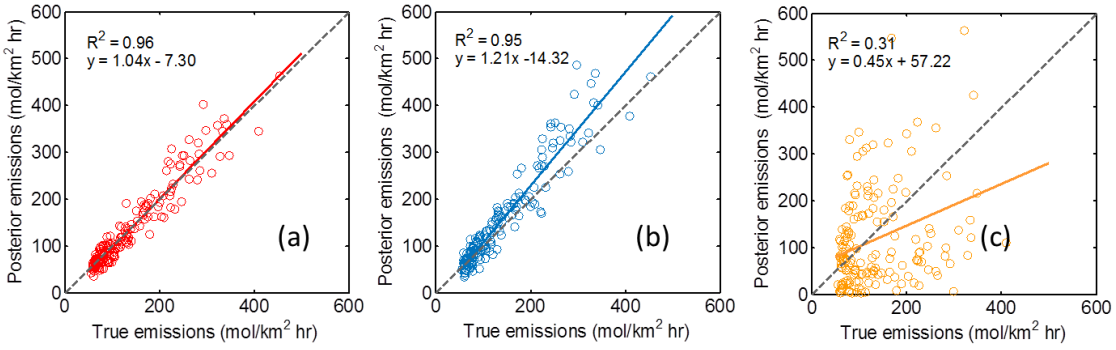

Figure 5. Comparison of posterior emission with true emission at the grid points with true emission above 50 mol/(km^2 hr). The 1:1 lines (dashed) and the linear regression lines (solid) are also shown. The regression parameters are shown in the inset. (a) ENS-H. (b) ENS-O. (c) BIAS-MET.

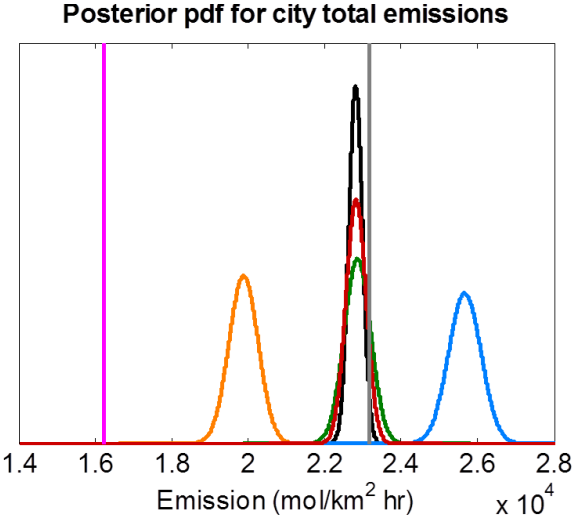

Figure 6. Probability distribution function (pdf) of city total emission in the posterior for REF (black), BIAS-MET (yellow), ENS-O (blue), ENS-T (green) and ENS-H (red). The magenta and grey lines represent the prior and true total emissions, respectively.